

Analysis of cluster explosive synchronization in complex networks

Peng Ji^{1,2,*}, Thomas K.D.M. Peron^{3,†}, Francisco A. Rodrigues^{4,‡} and Jürgen Kurths^{1,2,5}

¹*Potsdam Institute for Climate Impact Research (PIK), 14473 Potsdam, Germany*

²*Department of Physics, Humboldt University, 12489 Berlin, Germany*

³*Instituto de Física de São Carlos, Universidade de São Paulo, Av. Trabalhador São Carlense 400, Caixa Postal 369, CEP 13560-970, São Carlos, São Paulo, Brazil*

⁴*Departamento de Matemática Aplicada e Estatística,*

Instituto de Ciências Matemáticas e de Computação, Universidade de São Paulo,

Caixa Postal 668, 13560-970 São Carlos, São Paulo, Brazil

⁵*Institute for Complex Systems and Mathematical Biology,*

University of Aberdeen, Aberdeen AB24 3UE, United Kingdom

Correlations between intrinsic dynamics and local topology have become a new trend in the study of synchronization in complex networks. In this paper, we investigate in this paradigm the influence of topology on dynamics of networks made up of second-order Kuramoto oscillators. In particular, based on mean-field calculations, we provide a detailed investigation of the recently reported phenomena of cluster explosive synchronization (CES) [Phys. Rev. Lett. 110, 218701 (2013)], analysing the model in scale-free and small-world networks as a function of several topological properties. We show that, in contrast to scale-free networks, the transition to the synchronous state in small-world structures tends to be continuous as the probability of rewiring increases. These results complement the previous findings regarding CES and also fundamentally deepen the understanding of the interplay between topology and dynamics under the constraint of correlating natural frequencies and local structure.

PACS numbers: 89.75.Hc, 89.75.Kd, 05.45.Xt

I. INTRODUCTION

Synchronization of collective phenomenon plays a prominent role in science, nature, social life, and engineering [1–3]. Recently, much research has been devoted to investigate effects of network topology on synchronization. In particular, in the context of synchronization of dynamical systems in which the formalism of the master stability function [4] is applicable, it has been shown that the asymptotic behavior of the dynamics is entirely described by the spectral properties of a network. Using a mean-field approximation, it has been shown that Kuramoto oscillators undergo a second order phase transition to synchronization and the onset of synchronization is determined by the largest eigenvalue of the adjacency matrix [5].

Until very recently, only continuous synchronization transitions were known to occur in complex networks. However, Gomez-Gardenes et al. [6] reported the first observation of discontinuous phase synchronization transitions in scale-free networks, triggering further works on the subject [7–12]. Moreover the model presented in [6] shows a different kind of interplay between the connectivity pattern and the dynamics. The phenomenon of explosive synchronization was proved to be an effect exclusively due to the microscopic correlation between the network topology and the intrinsic dynamics of each os-

cillator. More specifically, the authors considered the natural frequencies of the oscillators to be positively correlated with the degree distribution of the network by assigning to each node its own degree as its natural frequency, rather than drawing it from a given symmetric distribution, as performed in previous works [13]. Discontinuous phase transitions were also previously observed in other dynamical processes in complex networks, such as in the context of explosive percolation in random [14] and scale-free [15, 16] networks. Similar to explosive synchronization, the explosive percolation has also a dynamical constraint related to the connectivity patterns, which is called the Achlioptas process [14].

Relevant to model several physical systems [17–20], the second-order Kuramoto model was also investigated under the constraint of correlation between natural frequency and degree distribution. In [21], we studied analytically and numerically how the inclusion of an inertia term in the equation for the phase evolution in the Kuramoto model would influence the network dynamics. Although the second-order Kuramoto model exhibits discontinuous synchronization transitions even in a fully connected graph for unimodal symmetric frequency distributions [18], a striking difference to the first-order Kuramoto model has been observed. By analyzing the average frequency $\langle \omega \rangle_k$ of each group of nodes with degree k , Gomez-Gardenes [6] found that nodes in scale-free networks join the synchronous component abruptly at the same coupling strength. In contrast, as shown in [21], the nodes perform a cascade of transitions toward the synchronous state grouped into clusters consisting of nodes with the same degree, a phenomenon called *cluster explosive synchronization* (CES) and also consisting in the

*Electronic address: pengji@pik-potsdam.de

†Electronic address: thomas.peron@usp.br

‡Electronic address: francisco@icmc.usp.br

first mean-field treatment of a second-order Kuramoto model in complex networks.

In spite of this new observed phenomena and all the attention that the paradigm of correlation between topology and dynamics has been attracting, here we extend the previous findings presented in [21]. More specifically, we analyze the parameter space for both branches in the hysteretic synchronization diagram, showing how the transition from a stable limit cycle to stable fixed points takes place as a function of the nodes degree and coupling strength. Furthermore, we also show that the critical coupling strength for the onset of synchronization, considering the adiabatic increasing of the coupling strength, decreases as a function of the minimum degree of the network. Finally, in order to compare with different topologies, we extend the results for Watts-Strogatz networks by tuning a single rewiring parameter $p \in [0, 1]$. A first-order phase transition appears for small p , while for large p , the first-order transition is not obvious. If the transition behavior to synchronization is obtained from the relaxation time, the time monotonically increases with p , which is a counter-intuitive result compared to [22].

This paper is organized as follows: In Sec. II we define the second-order Kuramoto model with correlation between the frequency and degree distributions in uncorrelated networks. Section III is devoted to the derivation of the self-consistent equations to calculate the order parameter as a function of the coupling strength in order to determine the synchronization boundaries in Sec. IV. In Sec. V we present our analytical and numerical results. Our final conclusions are developed in Sec. VI.

II. THE SECOND-ORDER KURAMOTO MODEL

A. model

The second-order Kuramoto model consists of a population of N coupled oscillators whose dynamics are governed by phase equations of the following universal form [21]:

$$\frac{d^2\theta_i}{dt^2} = -\alpha \frac{d\theta_i}{dt} + \Omega_i + \sum_{j=1}^N \lambda_{ij} A_{ij} \sin(\theta_j - \theta_i), \quad (1)$$

where θ_i is the phase of unit i ($i = 1, \dots, N$), α the dissipation parameter, Ω_i the natural frequency, λ_{ij} the coupling strength and A_{ij} an element of the network adjacency matrix \mathbf{A} , where $A_{ij} = 1$ if the oscillators i and j are connected and $A_{ij} = 0$ otherwise.

In a power grid modeled by the second order Kuramoto model, for example, the coupling λ_{ij} is proportional to the maximum power capacity of the transmission line between the nodes i and j [23]. Here, we consider that all connections have the same capacity and so we have a homogeneous coupling $\lambda_{ij} = \lambda$, $\forall i, j$. Ω_i can represent the power consumed (minus for consumers) or pro-

duced (positive for generators). Additionally, the sum of the consumed power is always equal to the produced power [24].

In order to get analytical insights on how the topology effects the dynamics, we assume that the natural frequency Ω_i of a node i is proportional to its degree according to

$$\Omega_i = D(k_i - \langle k \rangle), \quad (2)$$

where D is the strength of the connection between power and degree. In an analogy with power grid networks modelled by the second-order Kuramoto model, the choice of Ω_i as in Eq. (2) assumes that in scale-free topologies a high number of nodes play the role of consumers (nodes with $k_i < \langle k \rangle$) and nodes with high degrees play the role of power producers (nodes with $k_i > \langle k \rangle$). Note that the relation $\sum_j \Omega_j = 0$ is satisfied, which means that the total consumed power ($\Omega_i < 0$) is equivalent to the total generated power ($\Omega_i > 0$).

Substituting Eq. (2) in Eq. (1) we have [21]

$$\frac{d^2\theta_i}{dt^2} = -\alpha \frac{d\theta_i}{dt} + D(k_i - \langle k \rangle) + \lambda \sum_{j=1}^N A_{ij} \sin(\theta_j - \theta_i). \quad (3)$$

All oscillators try to rotate independently at their own natural frequencies, while the coupling λ tends to synchronize them to a common phase. The local connection between oscillators is defined by the adjacency matrix \mathbf{A} .

B. Mean field theory

In order to study the system analytically in the continuum limit, we define $\rho(k; \theta, t)$ as the density of oscillators with phase θ at time t , for a given degree k . It is normalized as

$$\int_0^{2\pi} \rho(k; \theta, t) d\theta = 1. \quad (4)$$

In uncorrelated complex networks, a randomly selected edge connects to the node with degree k and phase θ at time t with the probability $kP(k)\rho(k; \theta, t)/\langle k \rangle$, where $P(k)$ is the degree distribution and $\langle k \rangle$ the average degree. Thus, the continuum version of Eq. (3) becomes

$$\begin{aligned} \frac{d^2\theta}{dt^2} &= -\alpha \frac{d\theta}{dt} + D(k - \langle k \rangle) \\ &+ \frac{\lambda k}{\langle k \rangle} \int \int k' P(k') \rho(k; \theta', t) \sin(\theta' - \theta) d\theta' dk' \end{aligned} \quad (5)$$

In order to visualize the dynamics of the phases, it is natural to follow [25] and define the order parameter r as $re^{i\psi(t)} = \sum_i k_i e^{i\theta_i(t)} / \sum_i k_i$, where k_i is the degree of the node i and ψ the average phase. This order parameter is different from $re^{i\psi(t)} = \sum_i e^{i\theta_i(t)} / N$, which accounts for the mean-field in the fully-connected graph regime [26].

The order parameter r quantifies the phase coherence. For instance, if the initial values of θ and $\dot{\theta}$ are randomly drawn from a uniform distribution and each oscillator rotates at its intrinsic frequency, then $r \approx 0$. On the other hand, if the oscillators act as a giant synchronous component, we have $r \approx 1$.

In the continuum limit, the order parameter r can be expressed as

$$re^{i\psi} = \frac{1}{\langle k \rangle} \int \int P(k') k' \rho(k; \theta, t) e^{i\theta'(t)} d\theta' dk'. \quad (6)$$

Seeking to rewrite the continuum version in terms of the mean-field quantities r and ψ , we multiply both sides of Eq. (6) by $e^{-\theta}$ and take the imaginary part, obtaining

$$\ddot{\theta} = -\alpha \dot{\theta} + D(k - \langle k \rangle) + k\lambda r \sin(\psi - \theta), \quad (7)$$

which is the same equation that describes the motion of a damped driven pendulum.

In the mean-field character, each oscillator appears to be uncoupled from each other, and interacts with other oscillators only through the mean-field quantities r and ψ . Specifically, the phase θ is pulled towards the mean-phase ψ . In the case of positive correlation between frequencies and degree, we cannot set $\psi = 0$, since the frequency distribution is not necessarily symmetric.

In order to derive sufficient conditions for synchronization, we choose the reference frame that rotates with the average phase ψ of the system, defining $\phi(t) = \theta(t) - \psi(t)$. If $\dot{\phi}(t) = 0$, the oscillator is synchronized with the mean-field. Defining $C(\lambda r) \equiv (\dot{\psi} + \alpha \dot{\psi})/D$ and substituting the new variable $\phi(t)$ in the mean-field equation (7), we obtain [21]

$$\ddot{\phi} = -\alpha \dot{\phi} + D(k - \langle k \rangle - C(\lambda r)) - k\lambda r \sin \phi. \quad (8)$$

III. ORDER PARAMETER

The solutions of Eq. (8) exhibit two types of long-term behavior, depending on the size of natural frequency $D(k - \langle k \rangle - C(\lambda r))$ relative to $k\lambda r$. Naturally, in order to obtain sufficient conditions for the existence of the synchronous solution of Eq. (8), we derive the self-consistent equation for the order parameter r that can be written as the sum of the contribution r_{lock} due to the oscillators which are phase-locked to the mean-field and the contribution of non-locked drift oscillators r_{drift} ; i.e., $r = r_{lock} + r_{drift}$ [27].

A. Locked Order parameter

Let us assume that all nodes that have a degree in the range $k \in [k_1, k_2]$ are locked. These oscillators are characterized by $\dot{\phi} = \ddot{\phi} = 0$ and approach a stable fixed point defined implicitly by $\phi = \arcsin\left(\frac{|D(k - \langle k \rangle - C(\lambda r))|}{k\lambda r}\right)$,

which is a k -dependent constant phase. Correspondingly, $\rho(k; \phi, t)$ is a time-independent single-peaked distribution and

$$\rho(k; \phi) = \delta \left[\phi - \arcsin \left(\frac{D(k - \langle k \rangle - C(\lambda r))}{k\lambda r} \right) \right] \quad \text{for } k \in [k_1, k_2], \quad (9)$$

where δ is the Dirac delta function. Therefore, the contribution of the locked oscillators is expressed as

$$r_{lock} = \frac{1}{\langle k \rangle} \int_{k_1}^{k_2} \int P(k) k e^{i\phi(t)} \delta \left[\phi - \arcsin \left(\frac{D(k - \langle k \rangle - C(\lambda r))}{k\lambda r} \right) \right] d\phi dk \quad (10)$$

From the imaginary part of Eq. (10), we yield

$$0 = \frac{1}{\langle k \rangle} \int_{k_1}^{k_2} k P(k) \frac{D(k - \langle k \rangle - C(\lambda r))}{\lambda r} dk, \quad (11)$$

and from the real part,

$$r_{lock} = \frac{1}{\langle k \rangle} \int_{k_1}^{k_2} k P(k) \sqrt{1 - \left(\frac{D(k - \langle k \rangle - C(\lambda r))}{k\lambda r} \right)^2} dk. \quad (12)$$

We consider first a scale-free network with a degree distribution given by $P(k) = A(\gamma)k^{-\gamma}$, where $A(\gamma)$ is the normalization factor and $\gamma = 3$. Substituting the degree distribution $P(k)$ and applying the variable transformation $x = D(k - \langle k \rangle - C(\lambda r))/\lambda k r$, we obtain the following implicit equation for the contribution of the locked oscillators

$$r_{lock} = \frac{A(\gamma)}{2D\langle k \rangle} \left[\left(x(k_2) \sqrt{1 - x^2(k_2)} \right) + \arcsin x(k_2) - \left(x(k_1) \sqrt{1 - x^2(k_1)} + \arcsin x(k_1) \right) \right]. \quad (13)$$

B. Drift order parameter

We analyze the drifting oscillators for $k \in k_{drift} \equiv [k_{min}, k_1] \cup [k_2, k_{max}]$, where k_{min} denotes the minimal degree and k_{max} is the maximal degree. The phase of the drifting oscillators rotates with the period T in the stationary state, so that their density $\rho(k; \phi, t)$ satisfies $\rho \sim |\dot{\phi}|^{-1}$ [27]. As $\oint \rho(k; \phi) d\phi = \int_0^T \rho(k; \phi) \dot{\phi} dt = 1$, this implies $\rho(k; \phi) = T^{-1} |\dot{\phi}|^{-1} = \frac{\Omega}{2\pi} |\dot{\phi}|^{-1}$, where T and Ω are the time period and the oscillating frequency of the running periodic solution of ϕ [27]. After substituting $\rho(k; \phi)$ into Eq. (6), we get

$$r_{drift} = \frac{1}{2\pi \langle k \rangle} \int_{k \in k_{drift}} \int_0^T k P(k) \Omega |\dot{\phi}|^{-1} e^{i\theta(t)} \dot{\phi} dt dk. \quad (14)$$

Without loss of generality, we assume that $\dot{\phi} < 0$ for $k \in [k_{min}, k_1]$ and $\dot{\phi} > 0$ for $k \in [k_2, k_{max}]$. Thus the real part of equation (14) becomes

$$r_{drift} = \frac{1}{2\pi \langle k \rangle} \left(- \int_{k_{min}}^{k_1} + \int_{k_2}^{k_{max}} \right) \int_0^T k P(k) \Omega \cos(\phi) dt dk. \quad (15)$$

A perturbation approximation of the self-consistent equations enables us to treat Eq. (15) analytically. After performing some manipulations motivated by [27], we get

$$r_{drift} = \left(- \int_{k_{min}}^{k_1} + \int_{k_2}^{\infty} \right) \frac{-r k^2 \lambda \alpha^4 P(k)}{D^3 (k - \langle k \rangle - C(\lambda r))^3 \langle k \rangle} dk \quad (16)$$

Thus, the two self-consistent equations for the order parameter r ,

$$r = r_{lock} + r_{drift}, \quad (17)$$

are obtained from Eqs. (13) and (16).

IV. PARAMETER SPACE AND SYNCHRONIZED BOUNDARIES

It is known that systems governed by the equations of motion given by Eq. (8) present a hysteresis as λ is varied [27–29]. Therefore we consider the system's dynamics for two distinct cases: (i) Increase of the coupling strength λ . In this case, the system starts without synchrony ($r \approx 0$) and, as λ is increased, approaches the synchronous state ($r \approx 1$). (ii) Decrease of the coupling strength λ . Now the system starts at the synchronous state ($r \approx 1$) and, as the λ is decreased, more and more oscillators lose synchrony, falling into the drift state.

Next, we study the following problem: why do phase transitions occur for a continuously varying coupling strength? We illustrate the phase transitions using the parameter space of the pendulum. For convenience, we non-dimensionalize equation (8) by $\tau = \sqrt{k\lambda r} t$ [30], and set $\beta \equiv \alpha / \sqrt{k\lambda r}$ and $I \equiv D(k - \langle k \rangle - C(\lambda r)) / (k\lambda r)$, yielding the dimensionless version:

$$\frac{d^2\phi}{d\tau^2} + \beta \frac{d\phi}{d\tau} + \sin \phi = I. \quad (18)$$

The variable β is the damping strength and I corresponds to a constant torque (cf. a damped driven pendulum). Fig. 1(a) shows the bifurcation diagram in the $\beta - I$ parameter space of Eq. (18). There are three types of bifurcations [28]: homoclinic and infinite-period bifurcations periodic orbits, and a saddle-node bifurcation of fixed points. An analytical approximation for the homoclinic bifurcation curve for small β was derived using Melnikov's method [28, 31] and the curve is tangent to the line $I = 4\beta/\pi$.

Our change of time-scale allows us to employ Melnikov's analysis to determine the range of integration $[k_1, k_2]$ in the calculation of $r = r_{lock} + r_{drift}$.

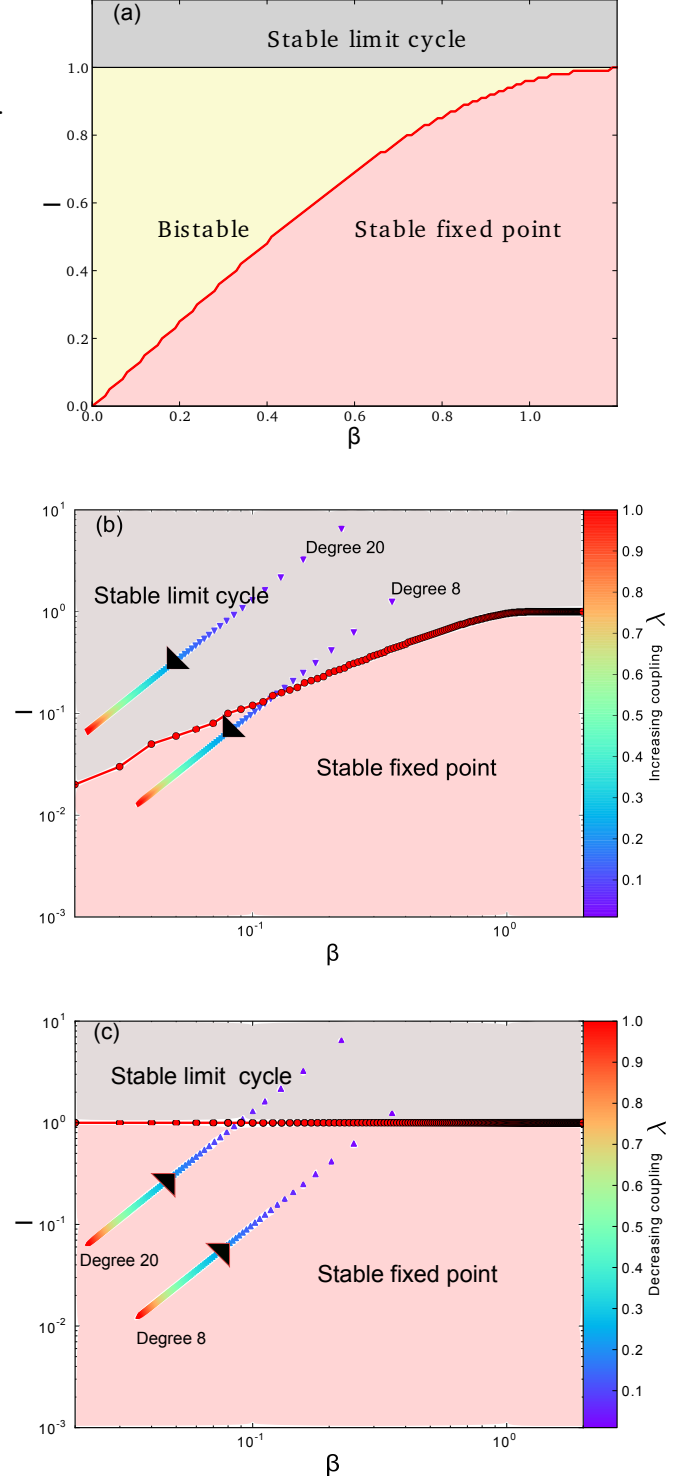


FIG. 1: (Color online). (a) Parameter space of the pendulum (Eq. (18)), (b) for increasing coupling strength and (c) decreasing coupling strength. The red area indicates the existence of a stable fixed point, whereas the gray area indicates the parameter combinations which give rise to a stable limit cycle. In the yellow area, oscillators either converge to the stable fixed point or rotate periodically depending crucially on initial conditions. Two schematic diagrams represent oscillators with degree $k = 8$ and degree $k = 20$, which start with incoherence in (b) (resp. coherence in (c)), and approach synchronous states (resp. incoherence), for increasing (resp. decreasing) coupling strength λ with $\alpha = 0.1$, $D = 0.1$, $\langle k \rangle = 10$, and $C = -3$.

A. Increasing coupling synchronized boundary

When the coupling strength λ is increased from λ_0 , the synchronous state emerges after a threshold λ_c^I has been crossed. Here we derive self-consistent equations that allow us to compute λ_c^I .

According to the stability diagram shown in Fig. 1(a) (derived from Eq. (18)), the parameter space is divided into three different areas corresponding to the stable fixed point, the stable limit cycle and bistability. The stable fixed point and the stable limit cycle coexist in the bistable area. Whether the oscillator will converge to the fixed point or rotate periodically depends crucially on the initial values of θ and $\dot{\theta}$ for given parameter values of β and I . As the coupling strength increases, the bistable area vanishes and we only get the stable limit cycle in this region. Thus the stability diagram is obtained (see Fig. 1(b)). Therefore, for $I > 1$, Eq. (18) has only one stable limit cycle solution. If $4\beta/\pi \leq I \leq 1$, the system is no longer bistable and only the limit cycle solution exists. If the coupling strength is increased further, the synchronized state can only exist for $I \leq 4\beta/\pi$, where Eq. (18) has a stable fixed point solution $\sin(\phi) = I$. Solving the inequalities

$$\frac{|D(k - \langle k \rangle - C(\lambda r))|}{k\lambda r} \leq 1, \quad (19)$$

and

$$\frac{|D(k - \langle k \rangle - C(\lambda r))|}{k\lambda r} \leq \frac{4\alpha}{\pi\sqrt{k\lambda r}}, \quad (20)$$

we get the following range of k^I for the phase-locked oscillators

$$k^I \in [k_1^I, k_2^I] = \begin{cases} \left[\frac{\langle k \rangle + C(\lambda r)}{1 + \lambda r}, \frac{\langle k \rangle + C(\lambda r)}{1 - \lambda r} \right] & \text{if } y < b, \\ \left[\frac{\langle k \rangle + C(\lambda r)}{1 + \lambda r}, K_2^I \right] & \text{if } b < y < 1, \\ [K_1^I, K_2^I] & \text{otherwise.} \end{cases} \quad (21)$$

Here, we define $b = \frac{16\alpha^2}{\pi^2(\langle k \rangle + C(\lambda r)) + 16\alpha^2}$ and

$$[K_1^I, K_2^I] \equiv \left[\frac{B - \sqrt{B^2 - 4D^4(\langle k \rangle + C(\lambda r))^2}}{2D^2}, \frac{B + \sqrt{B^2 - 4D^4(\langle k \rangle + C(\lambda r))^2}}{2D^2} \right],$$

where

$$B = 2D^2(\langle k \rangle + C(\lambda r)) + \frac{16\alpha^2\lambda r}{\pi^2}, \quad (22)$$

and $y \equiv \lambda r$. Since λr is present in all equations, we define a new variable y and analyze the self-consistent equations computing $r = y/\lambda$.

In order to visualize the dynamics and deepen the understanding of phase transitions, we sketch in Fig. 1(b) the phase trajectories of two randomly selected oscillators with degree $k = 8$ and 20. When the coupling strength is close to 0, the oscillators are in the stable limit cycle area and each node oscillates with their own natural frequency. One can see that the critical coupling for the onset of synchronization of the oscillator with degree $k = 8$ is lower and thus the small degree oscillator converges to the fixed point at lower coupling strength.

B. Decreasing synchronized boundary

With a decreasing coupling strength λ , the oscillators start from the phase-locked synchronous state, and reach the asynchronous state at a critical coupling λ_c^D . In order to calculate this threshold, we again investigate the range of degree k^D of the phase-locked oscillators. Imposing the phase locked solution in Eq. (8), we obtain $\sin \phi = \frac{|D(k - \langle k \rangle - C(\lambda r))|}{k\lambda r} \leq 1$ and find that the locked oscillators are the nodes with degree k in the following range as a function of λr

$$k^D \in [k_1^D, k_2^D] \equiv \left[\frac{\langle k \rangle + C(\lambda r)}{1 + \frac{\lambda r}{D}}, \frac{\langle k \rangle + C(\lambda r)}{1 - \frac{\lambda r}{D}} \right]. \quad (23)$$

This allows us to calculate r^D and λ_c^D from the self-consistent Eqs. (12) and (16).

Following the same procedure for increasing coupling strength, we also sketch phase trajectories of two oscillators with degree $k = 8$ and 20, respectively, in the parameter space as shown in Fig. 1(c). For high coupling strength, the population acts like a giant node and $r \simeq 1$. If $I < 1$, only a stable fixed point exists, whereas the oscillators rotate periodically. The oscillators with degrees $k \geq 20$ are easier dragged out of synchronization, For $I > 1$ the oscillators with degree $k = 20$ are easier to be out of synchronization compared to the ones with degree $k = 8$. In this way, the order parameter r would first slightly decrease and then abruptly drop to lower values.

V. ANALYTICAL RESULTS AND SIMULATIONS

A. Simulations on scale-free networks

We demonstrate the validity of our mean-field analysis by conducting numerical simulations of the second-order Kuramoto model with $\alpha = 0.1$ and $D = 0.1$ on Barabási-Albert scale-free networks characterized by $N = 3000$, $\langle k \rangle = 10$, $k_{min} = 5$ and the degree distribution $P(k) \sim k^{-\gamma}$, with $\gamma = 3$. Again, due to hysteresis, we have to distinguish two cases: First, we increase the coupling strength λ from λ_0 by amounts of $\delta\lambda = 0.1$, and compute the order parameter r^I for $\lambda = \lambda_0, \lambda_0 + \delta\lambda, \dots, \lambda_0 + n\delta\lambda$. Second, we gradually decrease λ from $\lambda_0 + n\delta\lambda$ to λ_0 in

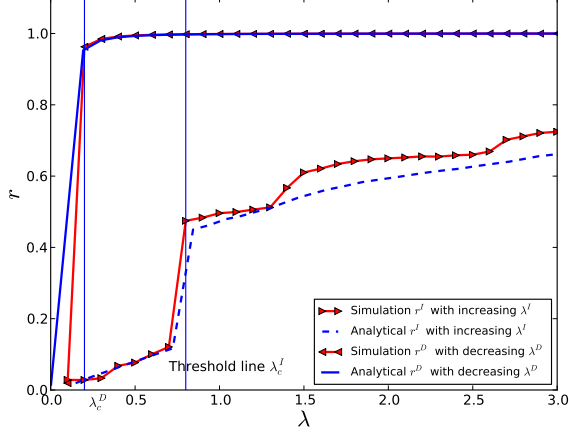


FIG. 2: (Color online). Analytical (in blue) and numerical (in red) analysis for synchronization diagrams. The analytical plots are calculated from Eqs. (13) and (16) with the synchronized boundary (21) for increasing coupling and (23) for decreasing coupling.

steps of $\delta\lambda$. Before each $\delta\lambda$ -step, we integrate the system long enough to arrive at stationary states.

Fig 2 shows the synchronization diagrams for the model defined in Eq. (3). The system exhibits the expected hysterical synchrony depending on initial conditions: In the case of an increasing coupling strength λ , the initial drifting oscillators can be entertained to locked oscillators after certain transience. The order parameter r remains at a low value until the onset of synchronization, λ_c^I , at which a first-order synchronization transition happens, and r increases continuously after that. In the case of decreasing λ , initially locked oscillators are desynchronized and fall into drift states once λ crosses λ_c^D . For a high coupling strength, all oscillators are synchronized and $r = 1$. As the coupling strength is decreased, the synchronized oscillators fall into unsynchronized states. As the two discontinuous transitions take place at different coupling thresholds, the order parameter exhibits hysteresis.

To validate our mean-field analysis with simulation results, we simultaneously solve Eqs. (13), (16) and (21) [resp. (13), (16) and (23)] for increasing [resp. decreasing] coupling strength. Note that the distribution of the natural frequencies is proportional to the degree distribution, and ψ can not be set 0 as has been done in previous works [32]. A key ingredient of the analytical process is $C(\lambda r)$ which we retrieve from the simulation data as shown in Fig. 3. Specifically, recalling that $C(\lambda r)$ depends on $\dot{\psi}$ and $\ddot{\psi}$, we assume that (i) $C(\lambda r) \approx 0$ (the blue solid curve in Fig. 3) when $\lambda < \lambda_c^I$, as each node oscillates at its own natural frequency, and (ii) $C(\lambda r) \approx \alpha\dot{\psi}/D$ when $\lambda \geq \lambda_c^I$. The oscillators with small degree synchronize first as shown in Fig. 7, and being in high percentage in a scale free network, they dominate

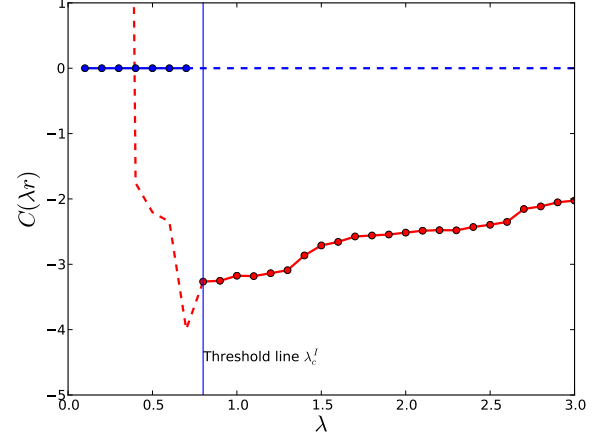


FIG. 3: (Color online). The simulation results with increasing coupling strength and $\langle k \rangle = 10$. The red line shows the mean value of $C(\lambda r) \simeq \alpha\dot{\psi}/D$. We take the value of $C(\lambda r)$ from the solid line in blue if $\lambda < \lambda_c^I$ and in red otherwise.

the mean field. The mean field rotates with a constant frequency $\dot{\psi}$ which we take from the simulations (the solid red line in Fig. 3). As before, it is convenient to analyze the system with $y \equiv \lambda r$ and $r = y/\lambda$. The analytical results are in good agreement with the simulations.

To deepen the understanding of the transition to synchrony, we calculate the average frequency of all oscillators of degree k [21], $\langle \omega \rangle_k = \sum_{[i|k_i=k]} \omega_i / (NP(k))$, where $\omega_i = \int_t^{t+T} \dot{\phi}_i(\tau) dt / T$ and t is large enough to let all oscillators reach stationary states. Fig. 4(a) shows that each cluster, an ensemble of oscillators with same degree, oscillates independently before the onset of synchronization. Oscillators with small degree, denoted by solid line, join the synchronous component simultaneously at λ_c^I . For further increasing coupling strength λ , more clusters, denoted by dashed lines, join the synchronized component successively, starting from small degrees, and correspondingly $C(\lambda r)$ becomes higher.

What happens inside each cluster at the onset of synchronization? We define the order parameter of each cluster denoted by $\langle r_k \rangle$, $\langle r_k \rangle = \int_t^{t+T} r_k dt / T$, where $r_k e^{i\psi_k} = \sum_{[i|k_i=k]} e^{i\theta_k} / (NP(k))$. When $\lambda < \lambda_c^I$ and initial values of θ are selected at random from $[-\pi, \pi]$, the oscillators of each cluster follow the same dynamics. Therefore, the oscillators are uniformly distributed over the limit cycle and $r_k \approx 0$ as shown in Fig. 4(b). The order parameter of the synchronized clusters denoted by solid line in Fig. 4 jumps to 1 at the onset of synchronization. After that, other clusters join the synchronized component and r_k approaches to 1 as denoted by the dashed lines.

In Fig. 5, we show the synchronized boundary $k^I \in [k_1^I, k_2^I]$ as a function of the coupling strength λ from the analytical and simulation results with increasing λ . The analytical and simulation results are in good agreement.

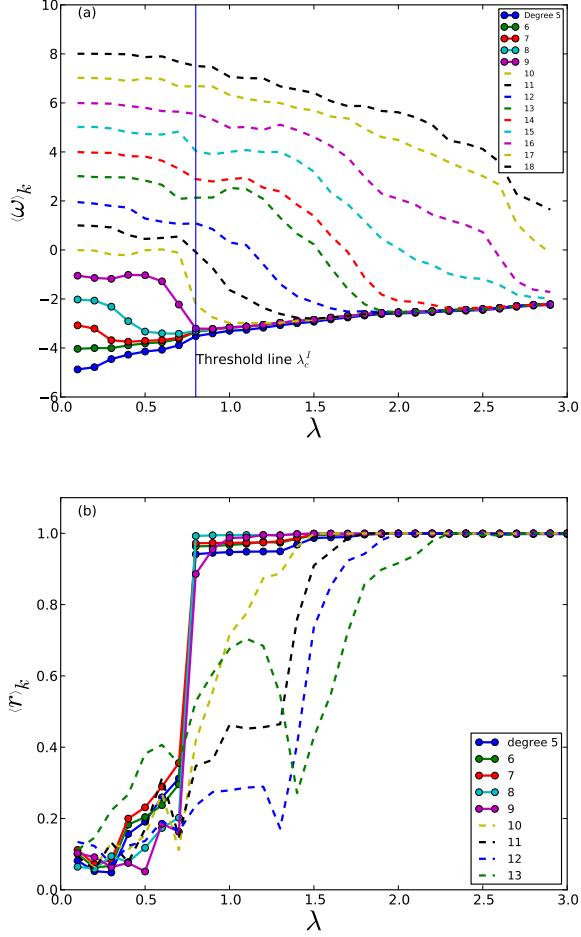


FIG. 4: (Color online). (a) Average frequency $\langle \omega \rangle_k$ and (b) order parameter r_k of each cluster from simulations with $\langle k \rangle = 10$. Solid lines denote synchronized clusters at the onset of synchronization. Dashed lines denote clusters with large degrees.

Note that the discontinuity of evolution of the synchronized boundary gives rise to a first-order phase transition in Fig. 2. After the transition to synchrony, the low boundary k_1^I stays constant at the minimal degree $k_{\min} = 5$, and, as more clusters join the synchronized component, the upper boundary k_2^I increases with λ .

The above results are based on scale free networks with the average degree $\langle k \rangle = 10$. To show more details, following the above process, we analyze the increasing coupling case with an average degree 12 with minimum degree $k_{\min} = 6$ as shown in Fig. 6. We integrate the equations (13), (16) and (21) and, by taking the values of $C(\lambda r)$ from the solid line of Fig. 6(a), we get the evolution of the order parameter r as a function of the coupling strength λ as shown in Fig. 6(b). We observe that the critical coupling strength in this case is smaller than that of scale-free networks with an average degree $\langle k \rangle = 10$.

We follow the above process again and investigate the

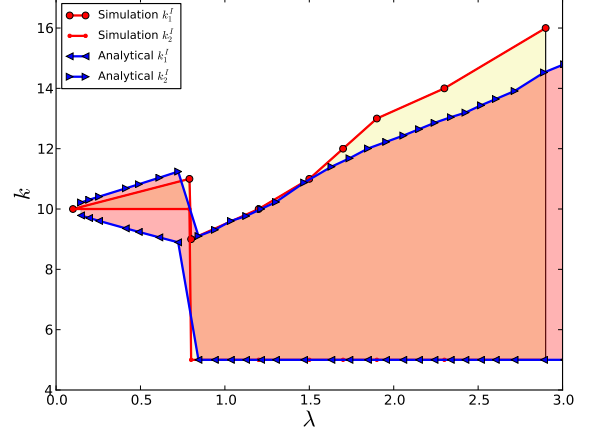


FIG. 5: (Color online). Synchronized degrees from analytical and simulations results with increasing coupling strength.

synchronization inside each cluster. As expected, initially oscillators for each cluster oscillate around its natural frequency and the order parameter r for each cluster remains at a low value (Fig. 7). Increasing the coupling strength further, a first-order transition to synchronization occurs at the threshold $\lambda_c^I = 0.6$. Clusters with a degree from $k = 6$ to $k = 10$ join the synchronization component simultaneously. More clusters join the synchronized component successively starting from low to high degrees.

It is natural to ask what is the influence of the average degree on the critical coupling threshold? Fig. 8 shows the mean threshold values of the critical coupling strength $\langle \lambda_c^I \rangle$ for increasing λ with different minimal degrees k_{\min} varying from $k_{\min} = 2$ to $k_{\min} = 20$. In simulations, if the difference between $r(\lambda)$ and $r(\lambda - \delta\lambda)$ is larger than, for example, 0.1, we define the transition to synchrony happens there. Due to the limitation of networks size, fluctuations of $\langle \lambda_c^I \rangle$ are unavoidable. The plots have been obtained with the same parameter values as above except minimal degrees k_{\min} . One can observe that the threshold values decrease with increasing minimal degrees initially and become almost constant afterwards.

B. Simulations on Watts-Strogatz networks

Previous studies of first-order transitions to synchronization with natural frequency correlated with degree are based on scale-free networks. Next, we also simulate the model in Eq. (3) on Watts-Strogatz networks by tuning the rewiring parameter $p \in [0, 1]$.

Synchronization appears when a tiny fraction of shortcuts comes into the system, moreover, the synchronizability increases with p as shown in [22]. Compared to these results, in Fig. 9, we observe counter-intuitive results

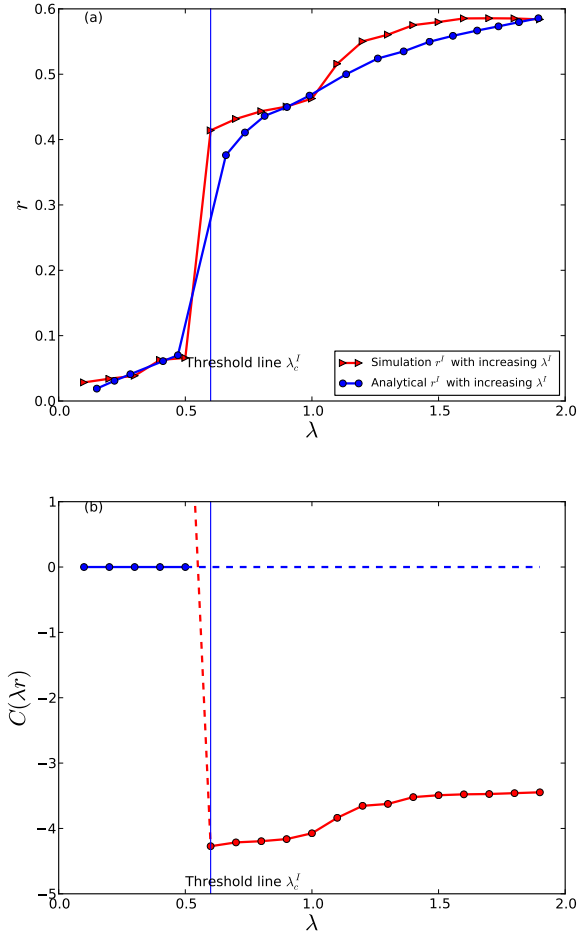


FIG. 6: (Color online). The results with increasing coupling strength λ . (a) shows the order parameter r vs. λ . The red (resp. blue) curve denotes the simulations (resp. analytical) results. (b) shows the $C(\lambda r)$ vs. λ . The critical coupling is 0.6. Same as in Fig. 3, we take the value from solid lines. Here the simulation is conducted with $\alpha = 0.1$, $D = 0.1$ and Barabási-Albert scale-free networks characterized by $N = 3000$, $\langle k \rangle = 12$, $k_{min} = 6$.

that the synchronizability decreases with the increasing of p . Synchronization exhibits strong dependence on the rewiring probability p . For small p , the system has a tiny fraction of short-cuts and most oscillators have a degree close to the average degree. Therefore, a high percentage of oscillators have a small natural frequency $D(k - \langle k \rangle)$ and tend to synchronize to the mean-field quantities already for a small coupling strength. For large p , due to the divergence of oscillators and large natural frequencies, the system needs a large coupling strength to recruit most oscillators into the synchronized component.

Fig. 10 shows the order parameter $\langle r \rangle_k$ of each cluster k with increasing coupling strength λ . The solid lines denote first-order transitions of clusters which join the synchronized component at the threshold. For small p , these clusters being in a high percentage produce first-

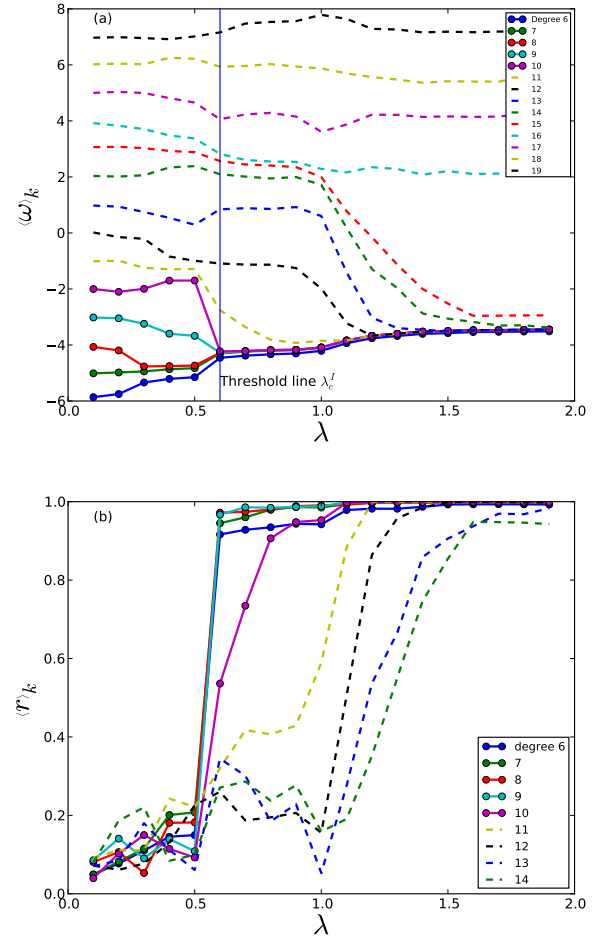


FIG. 7: (Color online). The results are got with the same parameter values of figure 6. (a) shows the evolution of the average frequency of each cluster $\langle \omega \rangle_k$ as a function of λ and (b) indicates the evolution of the order parameter of each cluster $\langle r \rangle_k$ of λ . Solid lines indicate the clusters synchronized at the critical threshold.

order transitions as shown in Fig. 9.

Correspondingly, one can see in Fig. 11(a) for $p = 0.1$, clusters with degrees from 8 to 10 synchronize to the zero mean-field value and other clusters join the synchronized component successively. Compared to small p , in Fig. 11(b), clusters join the synchronized component continuously.

VI. CONCLUSION

In summary, we have shown that the cluster explosive synchronization happens in the second order Kuramoto model with a correlation between natural frequency and degree. In previous studies on explosive synchronization, results have demonstrated that a first-order transition to synchrony is due to a position correlation between the local structure (degree) and the internal dynamics (nat-

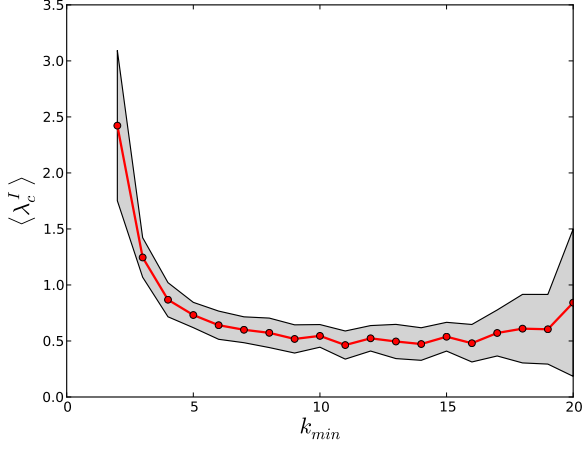


FIG. 8: (Color online). Mean threshold values of coupling strength $\langle \lambda_c^I \rangle$ for increasing coupling with different minimal degrees k_{min} . The grey shading indicates the standard deviation.

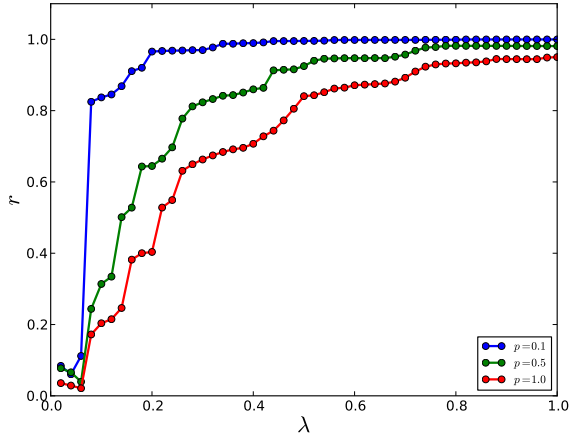


FIG. 9: (Color online). Order parameter r vs. coupling strengths λ for different p . Synchronizability decreases with p 's increase. A first-order phase transition is obvious for $p = 0.1$.

ural frequencies) of nodes. The synchronization diagram exhibits a strong hysteresis due to the different critical coupling strengths for increasing and decreasing coupling strength. As a function of the coupling strength, we have derived self-consistent equations for the order parameter, which is a sum of the locked order parameter and the drift order parameter. One of the key processes is to use a perturbation approximation to obtain the drift order parameter. The projection of the phase transition on the parameter space of a pendulum has enabled the derivation of the analytical expression of the synchronized boundaries for increasing and decreasing coupling strength. We have solved the self-consistent equation and the synchronized boundaries simultaneously, and the analytical re-

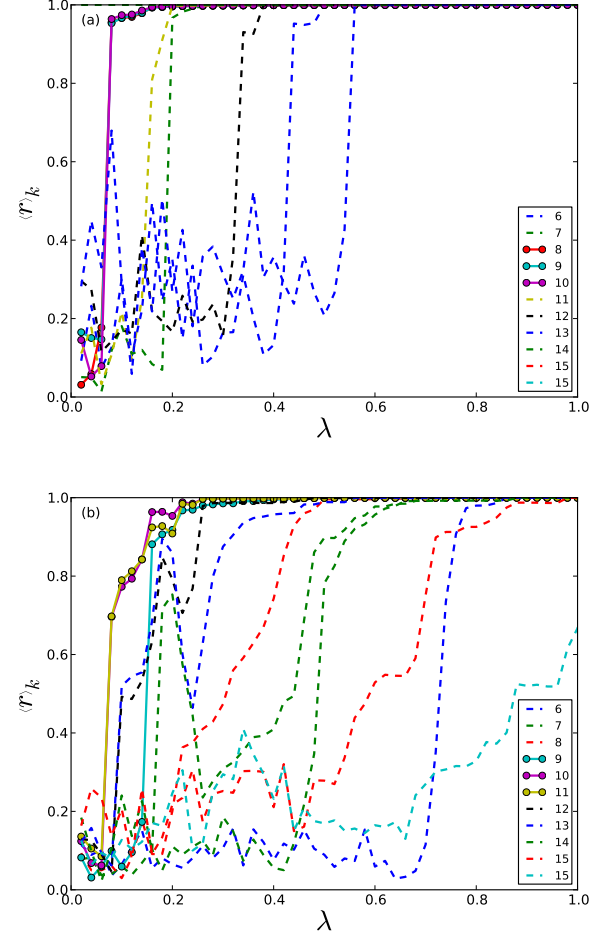


FIG. 10: (Color online). Order parameter of each cluster vs. coupling strengths λ for $p = 0.1$ and $p = 1$. Clusters with natural frequencies close to 0 tend to synchronize to the mean-field quantities at the threshold and first-order transitions of these clusters are represented by solid lines.

sults have been compared to the simulations and both show a good agreement. Shown numerically, the onset of synchronization for increasing coupling strength decreases with minimal degrees.

Following the previous processes, we have simulated the model on Watts-Strogatz networks and found a counter-intuitive phenomenon in which synchronizability decreases with the rewiring probability p . The order parameter and average frequency of each cluster have also been investigated for small and large p respectively.

The hysteresis in Barabasi-Albert scale-free networks with scaling exponent equal to $\gamma = -3$ has been investigated. However, it is an open issue what happens if the scaling exponent varies. Although hysteresis is a typical character of scale-free networks, the underlying mechanism for the occurrence of hysteresis in scale free networks (but not in random networks) remains open. The impact of topology on dynamics with more com-

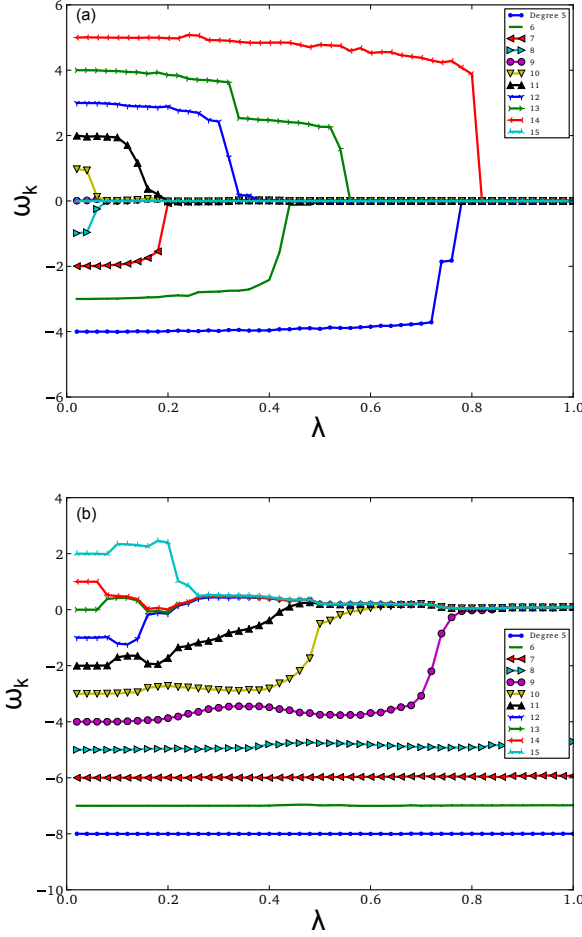


FIG. 11: (Color online). Average frequency of each cluster $\langle \omega \rangle_k$ vs. coupling strengths λ . In (a), for $p = 0.1$, clusters being in high percentage join in the synchronized component at the threshold and determine the 0 mean frequency. Other clusters join to the 0 mean-field afterwards according to the degree difference to the average degree. In (b), clusters join the synchronized component continuously.

plicated correlation between local topology and natural frequencies is also a subject for further work.

Acknowledgement

P. Ji would like to acknowledge China Scholarship Council (CSC) scholarship. T. Peron would like to acknowledge FAPESP (No. 2012/22160-7) and within the scope of IRTG 1740. F. A. Rodrigues would like to acknowledge CNPq (No. 305940/2010-4) and FAPESP (No. 2010/19440-2) for the financial support given to this research. J. Kurths would like to acknowledge IRTG 1740 (DFG and FAPESP) for the sponsorship provided.

-
- [1] A. Pikovsky, M. Rosenblum, and J. Kurths, *Synchronization: A universal concept in nonlinear sciences*, vol. 12 (Cambridge University Press, 2003).
 - [2] S. H. Strogatz, *Sync: The emerging science of spontaneous order* (Hyperion, 2003).
 - [3] A. Arenas, A. Díaz-Guilera, J. Kurths, Y. Moreno, and C. Zhou, Phys. Rep. **469**, 93 (2008).
 - [4] L. M. Pecora and T. L. Carroll, Phys. Rev. Lett. **80**, 2109 (1998).
 - [5] J. G. Restrepo, E. Ott, and B. R. Hunt, Phys. Rev. E **71**, 036151 (2005).
 - [6] J. Gómez-Gardeñes, S. Gómez, A. Arenas, and Y. Moreno, Phys. Rev. Lett. **106**, 128701 (2011).
 - [7] I. Leyva, R. Sevilla-Escoboza, J. M. Buldú, I. Sendiña Nadal, J. Gómez-Gardeñes, A. Arenas, Y. Moreno, S. Gómez, R. Jaimes-Reátegui, and S. Boccaletti, Phys. Rev. Lett. **108**, 168702 (2012).
 - [8] T. K. D. Peron and F. A. Rodrigues, Phys. Rev. E **86**, 016102 (2012).
 - [9] T. K. D. Peron and F. A. Rodrigues, Phys. Rev. E **86**, 056108 (2012).
 - [10] W. Liu, Y. Wu, J. Xiao, and M. Zhan, EPL (Europhysics Letters) **101**, 38002 (2013).
 - [11] X. Zhang, X. Hu, J. Kurths, and Z. Liu, Phys. Rev. E **88**, 010802 (2013).
 - [12] G. Su, Z. Ruan, S. Guan, and Z. Liu, EPL (Europhysics Letters) **103**, 48004 (2013).
 - [13] A. Arenas, A. Díaz-Guilera, J. Kurths, Y. Moreno, and C. Zhou, Phys. Rep. **469**, 93 (2008).
 - [14] D. Achlioptas, R. D'Souza, and J. Spencer, Science **323**, 1453 (2009).
 - [15] F. Radicchi and S. Fortunato, Phys. Rev. Lett. **103**,

- 168701 (2009).
- [16] Y. S. Cho, J. S. Kim, J. Park, B. Kahng, and D. Kim, Phys. Rev. Lett. **103**, 135702 (2009).
 - [17] M. Rohden, A. Sorge, M. Timme, and D. Witthaut, Phys. Rev. Lett. **109**, 064101 (2012).
 - [18] J. A. Acebrón and R. Spigler, Phys. Rev. Lett. **81**, 2229 (1998).
 - [19] F. Dorfler and F. Bullo, SIAM J. Contr. Optim. **50**, 1616 (2012).
 - [20] B. R. Trees, V. Saranathan, and D. Stroud, Phys. Rev. E **71**, 016215 (2005).
 - [21] P. Ji, T. K. D. Peron, P. J. Menck, F. A. Rodrigues, and J. Kurths, Phys. Rev. Lett. **110**, 218701 (2013).
 - [22] H. Hong, M. Y. Choi, and B. J. Kim, Phys. Rev. E **65**, 026139 (2002).
 - [23] G. Filatrella, A. Nielsen, and N. Pedersen, The European Physical Journal B-Condensed Matter and Complex Systems **61**, 485 (2008).
 - [24] J. Machowski, J. Bialek, and J. Bumby, *Power system dynamics: stability and control* (John Wiley & Sons, 2011).
 - [25] T. Ichinomiya, Phys. Rev. E **70**, 026116 (2004).
 - [26] Y. Kuramoto, *Chemical Oscillations, Waves, and Turbulence*, Dover Books on Chemistry Series (Dover Publications, 2003).
 - [27] H.-A. Tanaka, A. J. Lichtenberg, and S. Oishi, Physica D: Nonlinear Phenomena **100**, 279 (1997).
 - [28] H. Strogatz Steven, *Nonlinear Dynamics And Chaos: With Applications To Physics, Biology, Chemistry, And Engineering* (Addison-Wesley, Reading MA, 1994).
 - [29] H. Tanaka, A. Lichtenberg, and S. Oishi, Phys. Rev. Lett. **78**, 2104 (1997).
 - [30] S. Strogatz, *Nonlinear dynamics and chaos: with applications to physics, biology, chemistry and engineering* (Perseus Books Group, 2001).
 - [31] J. Guckenheimer and P. Holmes, *Nonlinear Oscillations, Dynamical Systems, and Bifurcations of Vector Fields*, vol. 42 (Springer-Verlag, Berlin, 1983).
 - [32] S. Strogatz, Physica D: Nonlinear Phenomena **143**, 1 (2000).